Chemical Physics Letters 593 (2014) 93–103

Contents lists available at ScienceDirect

Chemical Physics Letters

journal homepage: www.elsevier.com/locate/cplett

FRONTIERS ARTICLE

Exploiting classical decoherence in dissipative quantum dynamics: Memory, phonon emission, and the blip sum

Nancy Makri

Departments of Chemistry and Physics, University of Illinois, 600 S. Goodwin Avenue, Urbana, IL 61801, USA

ARTICLE INFO

Article history:
Available online 17 December 2013

ABSTRACT

The mechanisms that lead to the quenching of the coherence of a quantum system interacting with a dissipative environment are analyzed within the path integral/influence functional framework. Classical and quantum contributions are identified and linked to stimulated and spontaneous phonon emission processes. Three ways of exploiting decoherence in numerical calculations are discussed. The first is based on the decay of memory effects with time separation and leads to well-known iterative quasi-adiabatic propagator path integral (i-QuAPI) schemes. The other two mechanisms exploit the prominent role of classical decoherence. Removal of classical memory is possible through the introduction of auxiliary variables, leading to efficient and accurate quantum–classical path integral (QCPI) methods. A third way is proposed, which involves systematic corrections to the fully incoherent limit. An efficient procedure for summing all paths associated with 'blips' (short off-diagonal path pair segments) is described. The ideas are illustrated with numerical calculations of tunneling dynamics.

1. Introduction

Dynamical processes in the condensed phase are known to be drastically different from those of isolated molecular systems. Interaction with environments composed of many degrees of freedom tends to modify the dynamics of a system embedded in it, causing a change in the purity of its state, along with irreversible progression to thermal equilibrium. These behaviors are often characterized collectively as dissipative processes. If a particular property of the isolated (classical or quantum) system exhibits periodic oscillatory (often also referred to as 'coherent') dynamics, dissipative interactions tend to damp the amplitude of these oscillations, leading to quenched oscillations or even monotonic (often exponential) decay. These effects are captured in various phenomenological models, but have also been observed via analytical treatments and computer simulation.

Quantum effects, such as level structure, tunneling, or phase interference, often play an important role in the dynamics of a molecular system of interest. As a result, a detailed atomistic picture of condensed phase dynamics requires the solution of a many-body quantum mechanical problem, which remains an impractical task. However, much progress can be made using simplified descriptions of the environment or approximate treatments of the dynamics.

This letter focuses on the nature of decoherence and its role in the development of accurate, fully quantum mechanical treatments of the dynamics that are possible in the so-called system-bath or generalized spin-boson models, [1,2] which arise when the system's environment is replaced by fictitious harmonic degrees of freedom [3]. This extremely convenient simplification is often well justified and can be derived via rigorous theoretical procedures [4]. However, even when a complex many-body environment is replaced by a harmonic bath, calculation of the system's dynamical properties continues to present a very demanding task. The most appealing and efficient way to proceed is offered by Feynman's path integral formulation of time-dependent quantum mechanics [5,6]. In this, the quantum mechanical amplitude is expressed as a sum of phases along all paths that connect the initial and final points. This elegant prescription captures the essence of quantum interference familiar from Young's 'two-slit' experiment. When the system is coupled to a bath, the contribution of each path is augmented by an influence functional [7] that accounts for dephasing and leads to damping. In the case of a harmonic bath, these damping factors are available exactly via integrals of the bath's spectral density [8]. However, the influence functional is nonlocal in time, [7] such that its effects cannot be determined simply from the system's coordinates at a particular time but instead depend on each entire path of the system. This behavior, which is analogous to the presence of memory in the classical generalized Langevin equation, [9] represents the main obstacle in the numerical evaluation of the path integral because it obviates a simple iterative decomposition. For a system described in terms of m states or grid points, the number of paths required for propagation to N time steps is m^{2N}. It is thus clear that evaluation of the full sum over paths is impractical for $N >> 10$. Stochastic sampling of the paths [10,11] via Monte Carlo [12] methods, along with stationary

E-mail address: nmakri@illinois.edu

0009-2614/$ - see front matter © 2014 Elsevier B.V. All rights reserved.
http://dx.doi.org/10.1016/j.cplett.2013.11.064

phase filtering [13–17] and multilevel blocking techniques [18,19] can be successful for short times, but the dramatic phase cancellation leads to rapid growth of the statistical error with the number of propagation steps.

In spite of the proliferation of discretized Feynman paths, it is possible to overcome the exponential growth of computational effort required for the evaluation of the real-time path integral. The reason is that the influence functional memory eventually decays to zero, such that distant time points are practically uncorrelated [20]. This observation led to the first formulation of a numerically exact method capable of obtaining the dynamics of quantum dissipative systems for long times [20–27]. The method involves an iterative procedure based on a multi-time propagator (a tensor) that includes the coordinates of all explicitly correlated time points within the memory span [20–22]. The iterative nature of that algorithm leads to linear scaling with the total propagation time. In addition, a physically motivated partitioning of the Hamiltonian [28,29] allows large time steps, a discrete variable representation [30,31] (DVR) of the influence functional offers compact lattice representations of the paths, [32] while the use of energy-filtered propagators, [28,33,34] along with the damping arising from the influence functional, causes the majority of system paths to carry exponentially small weights. Path filtering procedures [24,35–37] can dramatically decrease the computational effort by retaining only statistically important path segments. By combining these advantages, the iterative quasi-adiabatic propagator path integral (i-QuAPI) methodology has found application to many processes in chemical and biological systems, while further advances have increased its efficiency [38–42] and generalized the approach to fermionic baths [43,44]. Although the iterative decomposition of the path integral was originally developed in the context of a system coupled to a harmonic bath, for which the influence functional is available analytically, it has been shown [45] that extension to anharmonic environments is possible [46,47] if the influence functional can be obtained by an efficient procedure. Additional path integral algorithms have also been reported in recent years, which utilize iterative [48] techniques and master equation hierarchies [49,50].

An interesting picture emerges if one considers the 'classical' limit of a high-temperature or low-frequency bath. Even though the influence functional is still nonlocal in general, it has been shown [51] that the nonlocality is removable in that limit, allowing replacement of the full path sum by the local dynamics of auxiliary variables. This property of the influence functional parallels a situation observed [52] in the context of a purely classical treatment of the bath *and* the system via the generalized Langevin equation [9] In the present context of the influence functional, the classical part (which is associated with the real part of the bath response function) gives rise to a *classical decoherence* mechanism, which involves the absorption and stimulated emission of phonons. This process dominates the evolution in cases of high-temperature or low-frequency baths, and even at low temperatures if the system-bath interaction is weak [53,54] In parallel with this classical decoherence, a *quantum decoherence* mechanism also affects the dynamics. This truly nonlocal process, which involves spontaneous phonon emission, is relatively insignificant at high temperatures, where classical decoherence dominates. At lower temperatures, the damping caused by the classical decoherence mechanism becomes less pronounced, allowing quantum decoherence to play a more prominent role.

The picture described above is not restricted to a harmonic bath. Even though no analytical expressions can be obtained for a complex polyatomic environment, it is still possible to obtain its influence functional numerically within semiclassical [55,56] or classical [57] approximations. These developments suggest a second way of exploiting decoherence and lead to a rigorous quantum–classical path integral (QCPI) formulation, in which all dynamical effects from the solvent are captured via classical trajectories [53,54,58]. Interestingly, the classical decoherence mechanism is associated with the trajectories of the solvent in the absence of interaction with the small quantum system [53]. These trajectories 'drive' the system, augmenting its Hamiltonian by a external potential that is local in time. The collective, ensemble-averaged effects of these trajectories give rise to damping. A quantum decoherence mechanism emerges from the so-called 'back-reaction', i.e. the perturbation of the solvent trajectories by the system, which is negligible in the high temperature limit. It is easy to see why the quantum decoherence process is nonlocal: As the system perturbs the trajectory of the solvent at every path integral time point, each system path gives rise to a distinct trajectory. Thus, the number of solvent trajectories required to account for quantum decoherence is proportional to the number of system paths, which grows rapidly with propagation time. This proliferation of trajectories can be terminated by recognizing that the effects of (classical and quantum) decoherence quench memory, thus only a finite length of nonlocality needs to be included explicitly [45,54].

This letter also shows that the above manifestations of classical decoherence can be exploited in yet another way, which can lead to a dramatic increase in the efficiency of path integral calculations with system-bath Hamiltonians. The main idea is that the bath-induced classical decoherence process tends to suppress quantum interference for the system [59–62]. As quantum interference arises from pairs of distinct forward and backward paths, the classical decoherence mechanism leads to the survival of path pairs that differ only over relatively short segments, the 'blips'. Some of these observations form the core of the noninteracting blip approximation [8] which established correctly the qualitative behaviors of the dissipative two-level system long before numerical methods were available. The present work exploits the rarity of blips to develop a systematic and efficient procedure for evaluating the full path integral. The blip sum method is ideally suited to the dynamics of systems coupled to sluggish baths, which are characterized by memory that spans several tens of time steps. These conditions present a challenge to path integral methods, and the i-QuAPI algorithm combined with path filtering may exhibit slow convergence in this regime.

Section 2 introduces the path integral representation of the density matrix, along with an overview of its cumulant expansion [4] which under certain conditions allows mapping of the influence functional from a complex many-body environment to the Gaussian influence functional corresponding to a harmonic bath. Iterative algorithms for evaluating the path integral, which are based on the finite span of influence functional memory, are reviewed in section 3. Section 4 discusses the classical and quantum origins of nonlocality, along with their dynamical consequences and the stimulated/spontaneous phonon emission mechanisms of decoherence they provide. Section 5 describes how the removal of memory that gives rise to classical decoherence can be exploited to enable rigorous and accurate quantum–classical path integral calculations for systems interacting with complex environments. Section 6 explores the blip-suppressing role of classical decoherence and describes the blip sum methodology, which converges rapidly to the exact path integral result. Some concluding remarks are given in Section 7.

2. Influence functional and the harmonic bath approximation

The interaction of a molecular system with its environment has the general form

$$H = H_0(\hat{s}, \hat{p}_s) + H_{\rm env}(\hat{s}, \hat{\mathbf{q}}, \hat{\mathbf{p}}) \tag{2.1}$$

Here H_0 is the Hamiltonian of the isolated quantum system, which is described by the coordinate(s) s, and $H_{\rm env}$ is the Hamiltonian for the system's environment, composed of many degrees of freedom with coordinates $\mathbf{q}$. For the purpose of studying the dynamics of the system without detailed knowledge of the state of the environment, it is useful to obtain the reduced density matrix,

$$\rho_{\rm red}(s_{\rm f}^{\pm};t)=\int d\mathbf{q}_{\rm f}\langle s_{\rm f}^{+}\mathbf{q}_{\rm f}|e^{-i\hat{H}t/\hbar}\hat{\rho}(0)e^{i\hat{H}t/\hbar}|s_{\rm f}^{-}\mathbf{q}_{\rm f}\rangle \tag{2.2}$$

where $\rho(0)$ is the initial density operator. Eq. (2.2) can also be written in the form

$$\begin{aligned}\rho_{\rm red}(s_{\rm f}^{\pm};t)=&\int ds_{\rm i}^{\pm}\int d\mathbf{q}_{\rm i}^{\pm}\int d\mathbf{q}_{\rm f}\langle s_{\rm f}^{+}\mathbf{q}_{\rm f}|e^{-i\hat{H}t/\hbar}|s_{\rm i}^{+}\mathbf{q}_{\rm i}^{+}\rangle\\&\times\langle s_{\rm i}^{+}\mathbf{q}_{\rm i}^{+}|\hat{\rho}(0)|s_{\rm i}^{-}\mathbf{q}_{\rm i}^{-}\rangle\langle s_{\rm i}^{-}\mathbf{q}_{\rm i}^{-}|e^{i\hat{H}t/\hbar}|s_{\rm f}^{-}\mathbf{q}_{\rm f}\rangle\end{aligned} \tag{2.3}$$

The first and third factors in the integrand are forward- and backward-time propagators. To proceed, it is convenient to express the propagators in path integral form. Adopting a time grid $t_k=k\Delta t$, where $\Delta t=t/N$ is the path integral time step, a discrete path of the system with fixed endpoints $s_{\rm i}^{-}\mathbf{q}_{\rm i}^{-}\equiv s_0\mathbf{q}_0$ and $s_{\rm f}\mathbf{q}_{\rm f}\equiv s_N\mathbf{q}_N$ is represented by the coordinates $\{s_0\mathbf{q}_0,s_1\mathbf{q}_1,\ldots,s_{N-1}\mathbf{q}_{N-1},s_N\mathbf{q}_N\}$. Summing over all such paths is equivalent to integrating with respect to all path coordinates, and one obtains the discretized path integral expression [6,63]

$$\begin{aligned}\langle s_N\mathbf{q}_N|e^{-i\hat{H}t/\hbar}|s_0\mathbf{q}_0\rangle=&\int ds_1\int d\mathbf{q}_1\cdots\int ds_{N-1}\\&\times\int d\mathbf{q}_{N-1}\langle s_N\mathbf{q}_N|e^{-i\hat{H}\Delta t/\hbar}|s_{N-1}\mathbf{q}_{N-1}\rangle\\&\times\cdots\langle s_2\mathbf{q}_2|e^{-i\hat{H}\Delta t/\hbar}|s_1\mathbf{q}_1\rangle\langle s_1\mathbf{q}_1|e^{-i\hat{H}\Delta t/\hbar}|s_0\mathbf{q}_0\rangle\end{aligned} \tag{2.4}$$

The main difference from Eq. (2.3) is that the propagators in the last expression involve short time increments, allowing approximate treatments. Without loss of generality, it is assumed that the Hamiltonian of the solvent with respect to which the thermal ensemble is defined corresponds to the coordinate $s=0$, and that the initial density matrix factorizes, i.e.,

$$\hat{\rho}(0)=\hat{\rho}_{\rm red}(0)\hat{\rho}_{\rm env}(0) \tag{2.5}$$

where for finite temperature processes

$$\hat{\rho}_{\rm env}(0)=\frac{e^{-\beta\hat{H}_{\rm env}(s=0)}}{{\rm Tr}\,e^{-\beta\hat{H}_{\rm env}(s=0)}} \tag{2.6}$$

with $\beta=1/k_{\rm B}T$. Factorization of the forward and backward short-time propagators according to the partitioning of Eq. (2.1) and integration with respect to all coordinates of the environment brings the reduced density matrix to the following form:

$$\begin{aligned}\rho_{\rm red}(s_N^{\pm};t)=&\int ds_0^{\pm}\cdots\int ds_{N-1}^{\pm}\langle s_N^{+}|e^{-i\hat{H}_0\Delta t/\hbar}|s_{N-1}^{+}\rangle\cdots\langle s_1^{+}|e^{-i\hat{H}_0\Delta t/\hbar}|s_0^{+}\rangle\\&\times\langle s_0^{+}|\hat{\rho}_{\rm red}(0)|s_0^{-}\rangle\langle s_0^{-}|e^{i\hat{H}_0\Delta t/\hbar}|s_1^{-}\rangle\cdots\langle s_{N-1}^{-}|e^{i\hat{H}_0\Delta t/\hbar}|s_N^{-}\rangle\\&\times F(s_0^{\pm},s_1^{\pm},\ldots,s_{N-1}^{\pm},s_N^{\pm})\end{aligned} \tag{2.7}$$

where

$$\begin{aligned}F(s_0^{\pm},s_1^{\pm},\ldots,s_{N-1}^{\pm},s_N^{\pm})=&\,{\rm Tr}_{\rm env}\,(\hat{U}_{\rm env}(s_0^{+},s_1^{+},\ldots,s_{N-1}^{+},s_N^{+})\hat{\rho}_{\rm env}(0)\\&\times\hat{U}_{\rm env}^{-1}(s_0^{-},s_1^{-},\ldots,s_{N-1}^{-},s_N^{-}))\end{aligned} \tag{2.8}$$

is the influence functional, [64] which incorporates all the effects of the environment on the dynamics on the system of interest. (Note that the functional terminology arises because in the exact representation of the propagators, i.e., in the limit $\Delta t\to 0$, the system paths are continuous functions of time; in the present case, where paths are labeled by a discrete time index, F is an ordinary function of the $2(N+1)$ path coordinates.) The operator $U_{\rm env}$ in Eq. (2.8) is the time evolution operator that corresponds to the Hamiltonian $H_{\rm env}$. It is useful to note that the parametric dependence of $H_{\rm env}$ on the path of the system makes this Hamiltonian explicitly time-dependent.

In the case of a complex polyatomic environment, such as a liquid or large biological molecule, it is presently impossible to calculate the influence functional by numerically exact, fully quantum mechanical methods. A very attractive possibility is to approximate it by accurate procedures based on classical trajectories [55–57,65]. However, an even more practical treatment is often adequate, and can be quantitative when the linear response approximation is valid. A rigorous derivation of this approximation and the conditions of its validity is based on a cumulant expansion of the influence functional [4]. This proceeds by expressing the latter in exponential form,

$$F\equiv\exp(\ln F) \tag{2.9}$$

and expanding the exponent in an infinite Taylor series,

$$\begin{aligned}F(s_0^{\pm},s_1^{\pm},\ldots,s_{N-1}^{\pm},s_N^{\pm})=\exp\Bigg(&\ln F_0+\sum_{k_1=0}^{N}\frac{\partial\ln F}{\partial s_{k_1}^{+}}s_{k_1}^{+}+\sum_{k=0}^{N}\frac{\partial\ln F}{\partial s_{k_1}^{-}}s_{k_1}^{-}\\&+\frac{1}{2}\sum_{k_1=0}^{N}\sum_{k_2=0}^{N}\frac{\partial^2\ln F}{\partial s_{k_1}^{+}\partial s_{k_2}^{+}}s_{k_1}^{+}s_{k_2}^{+}\\&+\sum_{k_1=0}^{N}\sum_{k_2=0}^{N}\frac{\partial^2\ln F}{\partial s_{k_1}^{+}\partial s_{k_2}^{-}}s_{k_1}^{+}s_{k_2}^{-}\\&+\frac{1}{2}\sum_{k_1=0}^{N}\sum_{k_2=0}^{N}\frac{\partial^2\ln F}{\partial s_{k_1}^{-}\partial s_{k_2}^{-}}s_{k_1}^{-}s_{k_2}^{-}+\cdots\Bigg)\end{aligned} \tag{2.10}$$

where the derivatives are evaluated at the point of expansion $s=0$, and $F_0=1$. Evaluation of the derivatives from the Dyson series representation of the influence functional shows that the coefficients of the various terms in Eq. (2.10) are given by equilibrium (multi-)time correlation functions of the force exerted on the system by the solvent [4]. For example, the quadratic (double sum) terms are given by the two-time force correlation function, the cubic terms (triple sum, not written explicitly in Eq. (2.10)) are given by the three-time correlation function, etc.

Evidently, the lowest order terms in Eq. (2.10) that are not equal to zero will dominate if the system-bath interaction is sufficiently weak. Interestingly, this is also the case if the interaction is spread uniformly over a large number of solvent degrees of freedom. Under this assumption, i.e., if

$$\frac{\partial}{\partial s}H_{\rm env}\bigg|_{s=0}=\sum_{j=1}^{n}c_j g(q_j), \tag{2.11}$$

and if the ensemble average of this vanishes at the expansion point, it can be shown [4] that *all* terms beyond quadratic order vanish in the $n\to\infty$ limit. Thus, the influence functional becomes

$$\begin{aligned}&F(s_0^{\pm},s_1^{\pm},\ldots,s_{N-1}^{\pm},s_N^{\pm})\\&=\exp\left(-\sum_{k=0}^{N}\sum_{k'=0}^{N}(\gamma_{kk'}^{++}s_k^{+}s_{k'}^{+}+\gamma_{kk'}^{+-}s_k^{+}s_{k'}^{-}+\gamma_{kk'}^{-+}s_k^{-}s_{k'}^{+}+\gamma_{kk'}^{--}s_k^{-}s_{k'}^{-})\right)\end{aligned} \tag{2.12}$$

where the coefficients are given by discretized forms of the solvent force autocorrelation function. Because of various symmetries, Eq. (2.12) can be written in the simpler form

$$F(s_0^{\pm},s_1^{\pm},\ldots,s_{N-1}^{\pm},s_N^{\pm})=\exp\left(-\sum_{k=0}^{N}\sum_{k'=0}^{k}(s_k^{+}-s_k^{-})(\eta_{kk'}s_{k'}^{+}-\eta_{kk'}^{*}s_{k'}^{-})\right). \tag{2.13}$$

In the limit $\Delta t \to 0$ the discrete time grid is replaced by a continuous variable and the sums in the influence functional are replaced by integrals, such that Eq. (2.13) becomes

$$F = \exp\left[-\frac{1}{\hbar}\int_0^t dt' \int_0^{t'} dt'' [s^+(t') - s^-(t'')][\alpha(t'-t'')s^+(t'') - \alpha(t'-t'')^* s^-(t'')]\right] \tag{2.14}$$

where α is the force autocorrelation function of the solvent, which is given by the expression

$$\alpha(t'-t'') = \sum_j \frac{c_j^2}{2m_j\omega_j}\left(\coth\left(\frac{1}{2}\hbar\omega_j\beta\right)\cos\omega_j(t'-t'') - i\sin\omega_j(t'-t'')\right) \tag{2.15}$$

Since under the stated conditions the influence functional has a Gaussian form, it can be mapped on the influence functional from a *fictitious* bath of harmonic oscillators. The mapping is performed by matching the force autocorrelation function of the effective bath to that of the true solvent. Specifically, the fictitious bath Hamiltonian has the form

$$H_b = \sum_j \frac{p_j^2}{2m_j} + \frac{1}{2}m_j\omega_j^2 x_j^2 - c_j s x_j \tag{2.16}$$

with a spectral density given by

$$J_\beta(\omega) \equiv \frac{\pi}{2}\sum_j \frac{c_j^2}{m_j\omega_j}\delta(\omega-\omega_j) = \frac{2}{\hbar}\tanh\left(\frac{1}{2}\hbar\omega\beta\right)\int_0^\infty \mathrm{Re}\langle \mathbf{f}(\mathbf{q}(0))\cdot\mathbf{f}(\mathbf{q}(t))\rangle_\beta \cos\omega t\, dt, \tag{2.17}$$

where $f = -\partial H_{\mathrm{env}}/\partial s$ and the subscript β implies a thermal equilibrium average. The spectral density determines completely the influence functional of the harmonic bath [8], thus Eq. (2.17) fully determines the harmonic bath that should under the above assumptions reproduce the effects on the system by the actual solvent. Under the specified conditions, the most complex environments are (as far as the system dynamics is concerned) exactly equivalent to the fictitious harmonic bath with the spectral density of Eq. (2.17). Note that the effective spectral density is temperature-dependent.

While the linear response assumption that allows mapping of a complex environment on that from a fictitious harmonic bath is not exact for a true molecular solvent or biological molecule, it appears to offer a very good approximation in cases of charge transfer dynamics, making Marcus' model of parabolic potential surfaces [3] usefully accurate. This is so because of the long-range nature of the Coulomb potential, which causes a very large number of solvent degrees of freedom to experience the interaction with the charge. The parabolic nature of the Marcus potential curves [3] is often justified in terms of the central limit theorem. Recent calculations have found mean-field potentials in crystals to be primarily harmonic [66]. For other processes (e.g., hydrogen atom transfer) the linear response approximation may provide a less successful picture, implying that no effective harmonic bath that adequately describes the dynamics can be identified. Apart from simulating specific molecular processes, the harmonic bath Hamiltonian has found extensive use as a generic model for studying the complicated interplay among tunneling, coherence and dissipation in condensed phase dynamics [1,2,8].

3. Memory and iterative decomposition of the path integral

The discretized path integral representation of a density matrix requires evaluation of a $2N$ -dimensional integral for each system degree of freedom. Full evaluation of such an integral represents a practically intractable task for $N >> 10$ even for a system described by a single coordinate. Many high-dimensional integrals are efficiently approximated by Monte Carlo methods [12,67] Unfortunately, this is not a very fruitful approach in the case of the real time path integral because the oscillatory real-time propagator leads to exponential growth of the statistical error [68,69]. For systems of just a few degrees of freedom, evaluation of the discretized path integral via simultaneous integration with respect to all variables is not only impractical but also unnecessary. This becomes apparent by examining the discretized path integral expression of the density matrix for the bare system,

$$\rho(s_N^\pm;t) = \int ds_0^\pm \cdots \int ds_{N-1}^\pm \langle s_N^+|e^{-i\hat{H}_0\Delta t/\hbar}|s_{N-1}^+\rangle \cdots \langle s_1^+|e^{-i\hat{H}_0\Delta t/\hbar}|s_0^+\rangle \times \langle s_0^+|\hat{\rho}(0)|s_0^-\rangle \langle s_0^-|e^{i\hat{H}_0\Delta t/\hbar}|s_1^-\rangle \cdots \langle s_{N-1}^-|e^{i\hat{H}_0\Delta t/\hbar}|s_N^-\rangle \tag{3.1}$$

Since each path integral variable appears only in adjacent propagators, the integrals in Eq. (3.1) may be evaluated sequentially via a series of matrix multiplications [70]. The iterative evaluation is a consequence of the underlying time-dependent Schrödinger equation (a first-order differential equation) which is entirely equivalent to the path integral.

The situation becomes more complicated when the path integral contains an influence functional. As seen in the previous section, the exponent of the influence functional from a harmonic bath, Eq. (2.13), involves a *double* sum which couples distant path integral variables. The loss of temporal locality is the result of the subspace representation, i.e., the replacement of the bath variables by the influence functional. The classical analogue of this situation is well known in the context of the generalized Langevin equation [9] (GLE), which also contains nonlocal terms commonly referred to as 'memory'. The entanglement of the path integral structure in the presence of the influence functional appears to obviate iterative procedures. However, the memory induced by the bath is in practice finite because the force correlation function that couples the two time variables eventually decays to zero for any bath that represents a condensed phase environment. The finite length $k - k' \equiv \Delta k_{\max}$ of the nonlocal influence functional interactions allows iterative evaluation of the path integral by propagating simultaneously all the time points that span the memory length [20]. The procedure involves a multitime density tensor which treats explicitly $\Delta k_{\max}$ time points. This is multiplied by a propagator tensor that spans $\Delta k_{\max} + 1$ time points and integrated with respect to the coordinates of the first time point to yield the multitime density tensor propagated by one time step [21,22]. The basic idea is illustrated in Figure 1. By arranging the path segments comprising the multitime density tensor in an array of $m^{2\Delta k_{\max}}$ elements, where m is the number of grid points employed in the discretization of the system coordinate, the procedure becomes a series of ordinary matrix multiplications. The iterative nature of the algorithm leads to linear scaling with the number N of propagation steps. This scaling represents dramatic computational savings, as full summation with respect to all paths would require m^{2N} operations. Many

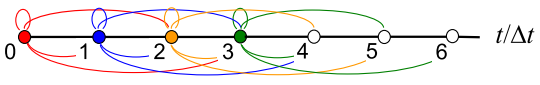

Figure 1. Diagrammatic representation of the influence functional couplings (curved lines) and the iterative propagation of the reduced density matrix in a case where the memory length is $\Delta k_{\max} = 3$ time steps. The circles indicate time points separated by Δt. Influence functional couplings originating from $k = 0, 1, 2$ and 3 are shown in red, blue, orange and green, respectively. Propagation of the 012 segment to the 123 segment is performed via multiplication by a propagator that contains all the red links and integration over the coordinates of the red point. Subsequently, multiplication by a propagator containing all the blue links and integration with respect to the coordinates of the blue point propagates to the 234 segment, etc.

problems of interest require propagation over thousands or even tens of thousands of time steps, thus iterative evaluation provides the only viable approach.

Still, the computational demands of the approach described above grow as $m^{2\Delta k_{\max}}$. It is thus desirable to use a time step as large as possible and (in cases where the system is described by a continuous coordinate) to minimize the number of required grid points. The path integral treatment involves factorization of the time evolution operator, but the traditional Trotter splitting [71] into kinetic and potential energy requires very small time steps for accuracy. The physically motivated quasi-adiabatic propagator [28] avoids splitting position and momentum terms, but also shifts the potential along the minimum energy valley (in a way reminiscent of a small polaron transformation [72]), achieving much larger time steps without increasing the complexity of the procedure. Calculation of the exact system reference propagators proceeds via an eigenstate expansion [28]. An additional benefit of that procedure is the smoothing offered by finite basis representations, which act as a filter, omitting high energy contributions responsible for the highly oscillatory behavior of conventional forms [33,34]. Last, system-specific discrete variable representations [31] (DVR) are employed [32] to discretize the system coordinates. These represent the most compact (sparse grid) representation that maintains a position-like character, a critical requirement for the simple expression of the influence functional.

The iterative quasi-adiabatic propagator path integral (i-QuAPI) methodology described above converges to the full path integral result. The only input required is the system Hamiltonian (either in terms of a continuous potential or in matrix form) and the bath spectral density [1], which may be specified numerically on a frequency grid from the Fourier integral given in Eq. (2.17). Thus, i-QuAPI offers a simple and efficient way of propagating the reduced density matrix, provided the bath induced memory is not very long (i.e., $\Delta k_{\max} \sim 10$). This is often the case when the bath includes a continuum of modes with frequencies that are high compared to the frequency components of the system. On the other hand, slow baths strongly coupled to the system often lead to memory that spans several tens of time steps. Direct implementation of the procedure described above becomes impractical in these cases. Progress is made by realizing that the vast majority of path segments that span the memory length make exponentially small contributions. Filtering procedures [24,35–37] discard the vast majority of path segments, retaining only those that are statistically significant. Such filtering techniques extend significantly the applicability of the i-QuAPI methodology to multi-level systems coupled to relatively slow solvents. The i-QuAPI methodology has produced useful benchmark results for spin-boson dynamics and barrier crossing, and been applied successfully to test the validity of analytic and numerical approximations, to investigate the interplay between tunneling, coherence and dissipation, and to study a host of proton, charge and energy transfer processes (for example, see references [73–89]. Its extension to include time-dependent fields is straightforward and has been used to investigate tunneling control [90–94] More recently, the methodology was generalized to include multiple bosonic and fermionic reservoirs [43,44].

Baths composed of strongly coupled fast and slow degrees of freedom present more challenging situations, as the high frequency oscillators enforce a small time step while the slow modes produce long-lived memory. An attractive way to proceed is renormalization of the propagator [40]. The main idea is to keep increasing the path integral time step successively, while including longer memory in each step of the process. While not exact, even the crudest two-time version of the renormalized propagator method often leads to nearly quantitative results. The algorithm can be made arbitrarily accurate by augmenting the scheme to a multitime propagator.

4. Classical vs. quantum decoherence, stimulated and spontaneous phonon emission

The bath alters the dynamics of the quantum system, allowing energy exchange and dephasing that cause an irreversible progression to equilibrium. By switching to sum and difference coordinates for the system,

$$\bar{s} = \frac{1}{2}(s^+ + s^-), \quad \Delta s = s^+ - s^- \tag{4.1}$$

the influence functional expression, Eq. (2.14), can be rewritten in the form

$$F = \exp\left(-\frac{1}{\hbar}dt' \int_0^t dt'' \int_0^{t'} dt'' \,\mathrm{Re}\alpha(t'-t'')\Delta s(t')\Delta s(t'')\right) \times \exp\left(-2\frac{i}{\hbar}\int_0^t dt' \int_0^{t'} dt'' \,\mathrm{Im}\alpha(t'-t'')\Delta s(t')\bar{s}(t'')\right) \tag{4.2}$$

It can be shown (see Eq. (4.7) below) that the double integral in the first term can be expressed as the sum of two squares. Thus, Eq. (4.2) shows that the real part of the response function leads to quenching of the quantum system's coherence.

To understand the nature of the decoherence process, it is instructive to consider the analogy with light absorption and emission. To this end, consider a classical treatment of the bath dynamics along a trajectory launched with initial phase space coordinates $\mathbf{x}_0, \mathbf{p}_0$. If the energy of this trajectory is sufficiently high, interaction with the quantum system will alter the course of the trajectory in minor ways. Neglecting such perturbations by the system, the coordinates of the bath trajectory are given by the relation

$$x_j(t) = x_{0j}\cos\omega_j t + \frac{p_{0j}}{m_j\omega_j}\sin\omega_j t \tag{4.3}$$

This motion 'drives' the dynamics of the quantum system, which is now governed by the time-dependent Hamiltonian

$$\hat{H}_0 - \sum_j c_j \hat{s} x_j(t). \tag{4.4}$$

The added time-dependent term modifies the dynamics of the system's density matrix, augmenting it by the phase [53].

$$\exp\left(\frac{i}{\hbar}\sum_j c_j x_{0j}\int_0^t dt'\Delta s(t')\cos\omega_j t' + \frac{i}{\hbar}\sum_j \frac{c_j p_{0j}}{m_j\omega_j}\int_0^t dt'\Delta s(t')\sin\omega_j t'\right). \tag{4.5}$$

Through this phase, each bath frequency component causes (in the long time limit) quantum transitions that correspond to the absorption or emission of one or more phonons (multiples of $\hbar\omega_j$). This picture is well-known in the context of molecule-light interaction, where a simple classical oscillating dipole treatment of the electromagnetic field is sufficient for deriving stimulated absorption and emission. Just as in the case of coherent light, the addition of the driving term in the Hamiltonian of Eq. (4.4) does not change the purity of the quantum system. However, in the present case where the bath is in a thermal ensemble, the phase given in Eq. (4.5) must be averaged with respect to the Boltzmann density,

$$P_{\mathrm{cl}}(\mathbf{x}_0, \mathbf{p}_0) = \prod_j \frac{\omega_j\beta}{2\pi}\exp\left(-\frac{1}{2}\beta m\omega_j x_{0j}^2 - \frac{\beta p_{0j}^2}{2m_j\omega_j}\right). \tag{4.6}$$

Performing the Gaussian integral and simplifying the result one finds that the bath modifies the system's density matrix by the factor

$$\exp\left(-\frac{c_j^2}{2m_j\omega_j^2\hbar\beta}\left(\int_0^t dt'\Delta s(t')\cos\omega_j t'\right)^2 - \frac{c_j^2}{2m_j\omega_j^2\hbar\beta}\left(\int_0^t dt'\Delta s(t')\sin\omega_j t'\right)^2\right) = \exp\left(-\frac{c_j^2}{m_j\omega_j^2\hbar\beta}\int_0^t dt'\int_0^{t'} dt''\Delta s(t')\Delta s(t'')\cos\omega_j(t'-t'')\right) \quad (4.7)$$

This shows that stimulated absorption and emission of phonons always leads to *quenching* of the system's coherence. The damping effects are most pronounced at high temperatures and increase as the ratio c_j/ω_j increases. However, Eq. (4.7) incorrectly predicts that the effects of the bath vanish in the limit of zero temperature. There are two reasons for this failure: First, the use of the classical Boltzmann distribution to obtain the thermal average cannot be expected to produce the correct result at low temperatures. Second, the free bath or 'classical path' approximation, i.e., the assumption that the bath trajectory is not perturbed by the system-bath interaction, breaks down at low temperatures, where small amplitude trajectories which are easily perturbed play the most important role.

It is easy to remedy the first of these flaws by replacing Eq. (4.6) by its quantum mechanical analogue, the Wigner [95] phase space transform of the Boltzmann operator,

$$P_{\rm qm}(\mathbf{x}_0,\mathbf{p}_0) = (\hbar\pi)^{-1}\tanh\left(\frac{1}{2}\hbar\omega_j\beta\right)e^{-\tanh(\frac{1}{2}\hbar\omega_j\beta)(m_j\omega_j x_j^2/\hbar + p^2/m_j\omega_j\hbar)}. \quad (4.8)$$

Use of this phase space density replaces Eq. (4.7) by the factor [53]

$$\exp\left(-\frac{c_j^2}{2m_j\omega_j\hbar}\coth\left(\frac{1}{2}\hbar\omega_j\beta\right)\int_0^t dt'\int_0^{t'} dt''\Delta s(t')\Delta s(t'')\cos\omega_j(t'-t'')\right) \quad (4.9)$$

which no longer vanishes in the zero-temperature limit. Thus, the corrected *ensemble-averaged classical path* (EACP) approximation of the bath dynamics captures the coherence quenching mechanism even at zero temperature. This behavior is a consequence of zero-point energy, which is enforced through quantization of the phase space density; specifically, the improved description of the bath's damping role through Eq. (4.9)–still obtained from the free bath trajectory approximation–arises from the zero-phonon state and thus corresponds to *spontaneous* phonon emission.

Eq. (4.9) is *identical* to the first factor of the influence functional in Eq. (4.2), which is obtained from the real part of the bath response function. Thus, this classical part of the response function, which grows rapidly with temperature, provides a (zero-point energy corrected) *classical decoherence* mechanism. In the high temperature/low frequency limit, i.e. when $\hbar\omega_j\beta\to 0$ for all bath degrees of freedom that couple significantly to the quantum system, the imaginary part of the response function is negligible in comparison with the real part and the classical decoherence mechanism dominates the dynamics.

On the other hand, the temperature-independent imaginary part of the response function contributes a pure phase. This part can modify the spectral characteristics of the evolution, but may also further dampen the system's oscillation amplitude by means of phase randomization. The EACP approximation cannot capture this contribution to the influence functional; thus the imaginary part of the response function provides a *quantum mechanical mechanism of decoherence*. This mechanism becomes important at low temperatures or when the bath includes strongly coupled high-frequency modes, which are primarily in their ground state. In these cases the real and imaginary parts of the response function have comparable magnitudes. Still, the role of the classical decoherence process is more prominent because of its direct damping effect.

The contributions of the classical and quantum decoherence mechanisms to the dynamics of a symmetric two-level system (TLS) are illustrated in Figures 2 and 3. The TLS Hamiltonian is given by the standard expression

$$H_0 = -\hbar\Omega\sigma_x \quad (4.10)$$

while the harmonic bath and TLS-bath interaction are given by

$$H_{\rm b} = \sum_j\left(\frac{p_j^2}{2m_j} + \frac{1}{2}m\omega_j^2x_j^2 - c_j\sigma_z x_j\right). \quad (4.11)$$

Here σ_x, σ_z are the Pauli spin matrices and the tunneling splitting of the bare TLS is $2\hbar\Omega$. The bath is described by the conventional Ohmic spectral density, [1]

$$J(\omega) = \frac{1}{2}\pi\hbar\xi\omega\, e^{-\omega/\omega_c} \quad (4.12)$$

which peaks at $\omega_c = 2.5\Omega$, while the Kondo parameter $\xi = 0.6$ indicates a moderate system-bath coupling strength. Three temperatures are considered: $k_{\rm B}T = 4\hbar\omega_c$, $k_{\rm B}T = 0.8\hbar\omega_c$ and $T\simeq 0$. The real part of the response function at these temperatures is shown in Figure 2, along with the temperature-independent imaginary part. The TLS is initially localized to site 1.

Figure 2 shows the time evolution of the reduced density matrix $\rho_{11}(t)$. In the first case, the bath degrees of freedom are at a high temperature. As a consequence, the classical decoherence mechanism reproduces the correct dynamics, giving rise to state populations indistinguishable from those obtained with the full influence functional. The additional damping arising from the imaginary part of the response function, which is independent of temperature, is inconsequential in this case, as the classical mechanism has already wiped out the oscillations in the TLS evolution. Classical decoherence continues to dominate the dynamics in the second case, where the bath has a moderately low temperature. In this case the consequences of the quantum decoherence mechanism, while minor, are clearly identifiable. Interestingly, the classical decoherence process still plays the most important role even in the third case where the bath is at zero temperature, although it does not by itself produce the correct TLS dynamics in this case.

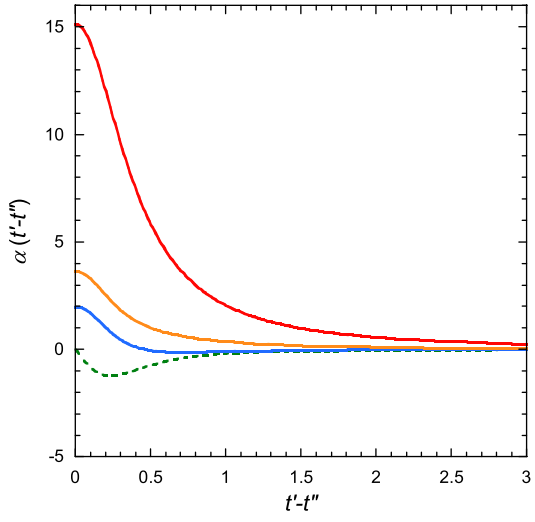

Figure 2. Response function for an Ohmic bath with $\omega_c = 2.5\Omega$, $\xi = 0.6$ at three temperatures. Solid red line: real part of the response function for $k_{\rm B}T = 4\hbar\omega_c$. Solid orange line: real part of the response function for $k_{\rm B}T = 0.8\hbar\omega_c$. Solid blue line: real part of the response function for $T\simeq 0$. Dashed green line: temperature-independent imaginary part of the response function.

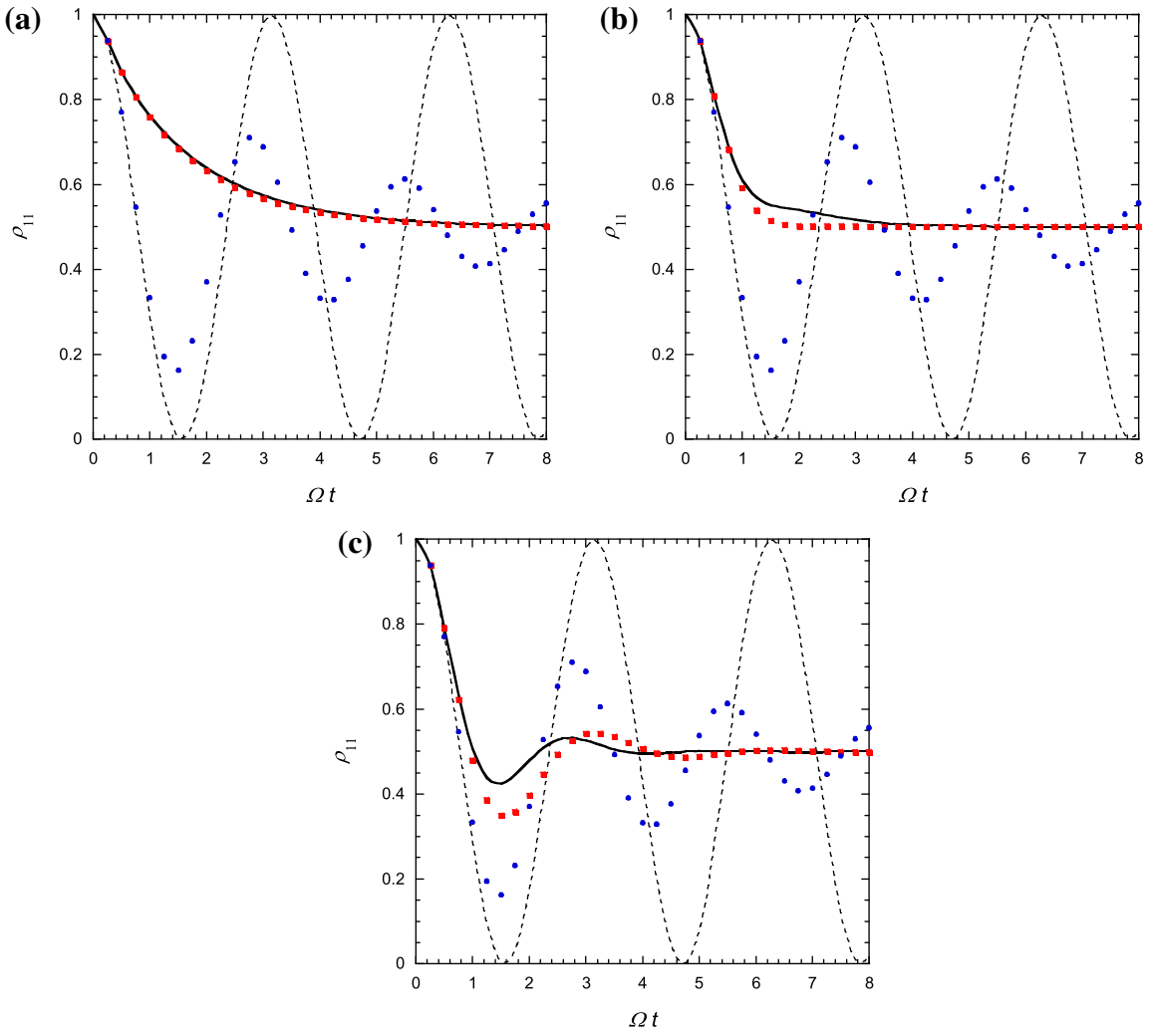

Figure 3. Population dynamics for a TLS coupled to an Ohmic bath with $\omega_c = 2.5\Omega$, $\xi = 0.6$. Solid black line: exact result, obtained with the i-QuAPI methodology. Dashed line: coherent population evolution for the bare TLS. Red markers: TLS dynamics subject to the classical decoherence process, obtained by using only the real part of the response function in the influence functional. Blue markers: TLS dynamics subject to the quantum decoherence process, obtained by using only the imaginary part of the response function in the influence functional. (a) $k_B T = 4\hbar\omega_c$. (b) $k_B T = 0.8\hbar\omega_c$. (c) $T \simeq 0$. In the last case the dissipative effects of the bath arise exclusively from the vacuum state; yet, the classical decoherence process captures the most important change in the dynamics even in this limit.

This is so because $\coth(\frac{1}{2}\hbar\omega\beta) \to 1$ as $T \to 0$, such that the real and imaginary parts of the response function have equal magnitudes, but the real part which leads to exponential damping has a much greater effect on the dynamics. Thus, the classical process captures the transition from coherent to underdamped dynamics, although not in a quantitative fashion, and inclusion of the residual quantum decoherence via the imaginary part of the response function is necessary to obtain the correct behavior in the low-temperature regime. The quantum decoherence mechanism is expected to become increasingly important also if the system-bath coupling is strong and/or if the population evolution is slow.

The nature of the quantum decoherence mechanism can be understood by considering the second reason for the low-temperature flaws of Eq. (4.7), namely the neglect of the 'back reaction' in the trajectory of the harmonic bath. It is not hard to show [53] that inclusion of the perturbation of the classical trajectory from the force exerted on it by the system recovers exactly the second influence functional factor in Eq. (4.2), which corresponds to the nonclassical, imaginary part of the response function.

The behaviors identified above are familiar from light emission. This is best seen by repartitioning the response function,

$$\alpha(t'-t'') = \sum_j \frac{c_j^2}{2m_j\omega_j}\left[\left(\coth\left(\frac{1}{2}\hbar\omega_j\beta\right)-1\right)\cos\omega_j(t'-t'') + e^{-i\omega_j(t'-t'')}\right] \tag{4.13}$$

The first term in this is still dominant as $T \to \infty$, but its contribution now vanishes in the zero temperature limit. The second term in Eq. (4.13), $\exp(-i\omega_j(t'-t''))$, arises exclusively from the contribution of the ground (zero-phonon) state, which in the context of light is associated with spontaneous emission. (In fact, one can derive the stimulated and spontaneous emission processes by examining the influence functional from the radiation field; the resulting expression has the form of Eq. (4.2), although the coefficient of the classical term, which coincides with the result of the classical oscillating dipole treatment, depends on the photon number rather than the temperature in the case of coherent light [96].) Note that the real part of this term, which causes exponential quenching and thus constitutes the most important dissipative effect of the vacuum, is contained in the EACP approximation, Eq. (4.9) that was obtained with a properly quantized density. This effect is illustrated very clearly in Figure 2, which shows that the EACP treatment reproduces at zero temperature the bulk of the tunneling oscillation quenching induced by the bath. The above

analysis shows that the traditional process of spontaneous (photon or phonon) emission has two contributions: one that arises from zero-point motion and is included in the quantized EACP approximation and one of a purely dynamical nature, which is associated with the 'back reaction'.

To summarize the above analysis, the 'classical' decoherence mechanism defined through Eq. (4.9) captures not only the stimulated absorption/emission effects associated with bath excitations, but also the most important contribution from spontaneous phonon emission processes. This feature generally makes classical decoherence the most prominent bath-induced effect on the dynamics of a quantum mechanical system.

5. Removal of classical memory and quantum–classical path integral

It has been shown [51] that the influence functional nonlocality associated with the real part of the response function, which is associated with classical decoherence, is removable at the cost of introducing auxiliary variables. This is seen most transparently from the treatment of the previous section, where the main effects of the bath on the system arise from unperturbed trajectories that 'drive' the system dynamics. Propagation of the system under the resulting time-dependent Hamiltonian (which is different for each trajectory initial condition) provides an efficient, memory-free propagation procedure that (upon averaging with respect to the trajectory initial conditions) captures all the bath effects associated with classical decoherence. As seen from the model calculations of Figure 3, the EACP approximation tends to be very accurate at high temperature and semi-quantitative at moderately low temperatures, where it even accounts for the most serious effects from spontaneous phonon emission.

Corrections are obtained by incorporating the EACP approximation in quantum–classical path integral (QCPI) expressions. This is achieved by replacing the system propagators in Eq. (2.7) by propagators that follow the dynamics of the time-dependent Hamiltonian (4.4), which includes the driving term obtained from a free bath trajectory [58]. At high temperatures and/or with low-frequency baths, where the EACP approximation is quantitative, no time slicing of the path integral is necessary. Under less favorable conditions, the EACP approximation gradually deviates from the exact result as the propagation time increases. By adjusting the number N of path integral time slices, the time length of the propagators is shortened, until the EACP approximation becomes sufficiently accurate within each path integral time step. The trajectory of the bath is now integrated subject to forces from the system, which are different at each path integral time point. Thus, each path of the quantum system gives rise to a different bath trajectory. The interference among these trajectories, which include the 'back reaction', corrects the shortcomings of the EACP approximation, accounting for the quantum mechanical mechanism of decoherence. The procedure may be combined with path filtering and may be generalized to an iterative algorithm in the spirit of the approach discussed in Section 3 [53].

QCPI formulations result from classical trajectory treatments of the solvent, whose forward and backward time evolution operators correspond to time-dependent Hamiltonians that include the interaction with the system along its particular forward and backward path pair. Most practical for implementation are the full forward–backward semiclassical dynamics (FBSD) formulation of the influence functional [55,56] and the linearized semiclassical approximation [57]. The latter follows from application of the linearized semiclassical initial value representation [97] or linearized path integral [98] approximation to the solvent dynamics and uses the Wigner phase space transform [95] of the initial density, while the solvent trajectories evolve subject to the average of the system forces along the forward and backward paths. The FBSD expression propagates the solvent trajectories with separate forces along the forward and backward paths, and is derived from the Herman–Kluk semiclassical approximation [99] that is based on the coherent state transform of the density, which may be evaluated via imaginary time path integral [65,100] or semiclassical [101] procedures. Both treatments produce exact quantum mechanical results in the case of a harmonic bath. Thus, QCPI offers another way of computing the evolution of quantum dissipative systems, which may be advantageous in cases of low-frequency, long-memory baths.

However, the main advantage of QCPI is in connection with anharmonic environments. The concepts of classical and quantum decoherence discussed in the previous section are completely general: Trajectories of the solvent, free of any dynamical perturbations by the system, drive the dynamics of the latter, giving rise to quantum transitions analogous to phonon absorption and emission via a classical decoherence mechanism. Propagation of the system in the presence of this time-dependent term is memory-free, thus straightforward. The results of this treatment constitute the EACP approximation, which can be corrected by including the back-reaction via a full path integral. The phase interference in this sum includes the effects of the quantum decoherence mechanism. Note that for $N > 1$, a classical trajectory feels the force determined by the coordinate (or state) of the system at the particular path integral time point. In the case of a TLS where the two sites represent states of different charge, the EACP approximation corresponds to a trajectory that evolves on a fixed charge state, while a full QCPI calculation includes state switches. Thus, QCPI is somewhat reminiscent of surface hopping algorithms [102,103], although there are several important differences; these include inclusion of all statistically significant state hops, which occur at regular intervals, the absence of velocity rescaling, as well as the absence of additional decoherence besides that which arises naturally via the mechanisms discussed above.

Application to spin-boson models and fully atomistic simulations of charge transfer in solution suggest that the QCPI methodology is sufficiently practical for application to many chemical and biological processes.

6. Exploiting classical decoherence:The blip sum

As is clear from the previous section, temperature scales (in a nonlinear way) the real part of the response function without affecting its shape. According to Eq. (4.2), this classical decoherence term plays the most important role as long as the forward and backward paths of the system are not identical at all times. At the same time, when the forward and backward system paths differ over large time intervals, the double time integral becomes large in absolute value, making the contribution of such path pairs exponentially small. This behavior is particularly prominent at high temperatures and/or with a classical-like, low-frequency bath, where the hyperbolic cotangent factor multiplying the integrated path difference is large. Thus, interaction with a classical reservoir suppresses quantum inteference effects by forcing the forward and backward paths of the system to be nearly identical, localizing the reduced density matrix. These ideas are well appreciated and have been observed in semiclassical calculations [104–106]. They are also very similar to the coherence quenching effects of thermal noise applied directly to the system [61,107].

Both numerical procedures reviewed in the previous sections, i.e. the i-QuAPI and the QCPI method, proceed by adding the dissipative effects of the environment to the *fully coherent* dynamics of the system. For this reason, both methods converge most rapidly

when the system-bath interaction is relatively weak, as the influence functional corrections to the evolution of the bare system are relatively minor in this case. By building the classical decoherence mechanism in the memory-free dynamics of the system, QCPI also converges with large time steps when the quantum decoherence contributions are small. However, the suppression of quantum interference by a nearly classical environment suggests that the *fully incoherent* limit may offer a better starting point for both methods. This limit corresponds to the bare system dynamics arising from identical forward and backward paths, i.e., the assumption that the density matrix remains diagonal at all times.

In this framework, the most significant corrections to the fully incoherent limit arise from path pairs that differ over relatively short time lengths. Leggett et al. [8] have adopted the term 'blips' for regions of $\Delta s \neq 0$. To be precise, I will use the term *blip* as a segment of a forward–backward path pair that spans a single path integral time step Δt. Segments of path pairs where the forward and backward coordinates are identical are called 'sojourns'. Blips may be consecutive or separated by several time steps (see Figure 4). The fully incoherent limit corresponds to path pairs with no blips.

According to Eq. (4.9), classical decoherence involves interactions between blips. Because the real part of the response function always decays in the vicinity of $t = 0$, the most important term in the discretized influence functional is the self-interaction from each of the blips, $-\mathrm{Re}\alpha_{kk}\Delta s_k^2$. Interblip terms generally become smaller with increasing time separation. However, classical baths tend to have long-lived response functions, implying that long memory effects must be included in the path integral. In light of the above discussion, such long-distance interactions between blips can be important, even though the number of blips in a particular path pair may be very small. Finally, quantum decoherence comes from blip-sojourn terms. These interactions are illustrated in Figure 5.

These observations can be exploited in path integral calculations with strongly coupled, low-frequency baths, for which the memory often spans several tens of time steps. Full summation would require inclusion of m^{2N} paths, which for $m = 2$ is easily feasible only up to $N \simeq 10 - 15$. The starting point is classification of path pairs in terms of the number ℓ of blips they contain. Under the stated conditions and for moderate propagation times, convergence is reached with path pairs containing only up to $\ell = 3 - 10$ blips. This number is typically much smaller than the number of time steps required to reach the desired propagation time or to span the influence functional memory. Thus, recognizing that paths with many blips have exponentially small weights eliminates a very large number of the m^{2N} paths. However, the number of remaining paths is still very large; for example, even the number of path pairs that contain no blips is m^N.

It is possible to evaluate the path sum in a much more efficient manner by observing that for each arrangement of the blips, the influence functional contains a single summation index and thus becomes local. This allows evaluation of the sum with respect to all sojourn segments between blips via efficient iterative procedures.

As an example, consider again a symmetric TLS coupled to a slow bath described by the spectral density of Eq. (4.12) with $\omega_c = 0.5\ \Omega$ and $\xi = 2$ at a temperature $T = 10\hbar\Omega$. These parameters correspond to long memory and thus represent a challenging regime. Figure 6 shows the population of the initial state, obtained with the blip sum procedure with $\ell = 0, 1, \ldots, 7$. While the decay is incoherent, it is not exponential because of the sluggish nature of the bath dynamics. It is seen that inclusion of path pairs with up to 4 blips yields results accurate through $\Omega t \simeq 2.5$, while results obtained with 6 blips are converged through $\Omega t \simeq 7.5$. The calculation with $\ell = 7$ gave results accurate until the populations have reached their equilibrium value of 0.5. In the present case, this involved propagation to $N = 50$ time steps without resorting to memory-truncating iterative algorithms. All calculations were performed on a single-processor laptop within a few hours.

As briefly mentioned in Section 3, path filtering provides an efficient full-memory approach for evaluating the path integral with large values of N. Since the omission of paths with weights larger than the acceptable threshold would affect the accuracy of the result, it follows that the blip sum method should not include a smaller number of paths than those identified automatically by the path filtering calculation. In fact, the blip sum method effectively includes *more* paths, because it accounts for *all* sojourn segments regardless of their weight. However, the blip sum method sums over sojourn segments using efficient iterative procedures and thus does not treat them explicitly. For example, a path of length $N = 50$ that contains 7 blips has sojourn segments of total length 43. For a TLS, there are 2^{43} possible arrangements of these sojourn

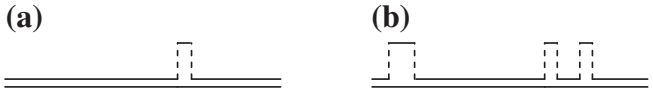

Figure 4. The Δs coordinate of two representative forward–backward path pairs. (a) Path pair with a single blip. (b) Path pair with four blips, two of which are consecutive.

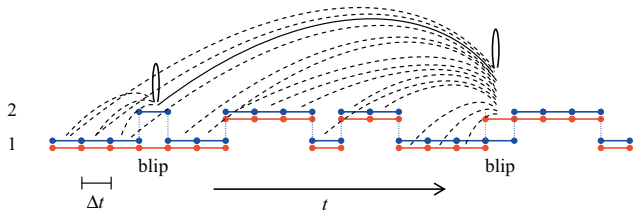

Figure 5. Blip–blip (solid curves) and blip–sojourn (dashed curves) interactions for a pair of forward–backward paths (shown in red and blue) with $N = 20$ time steps and two blips.

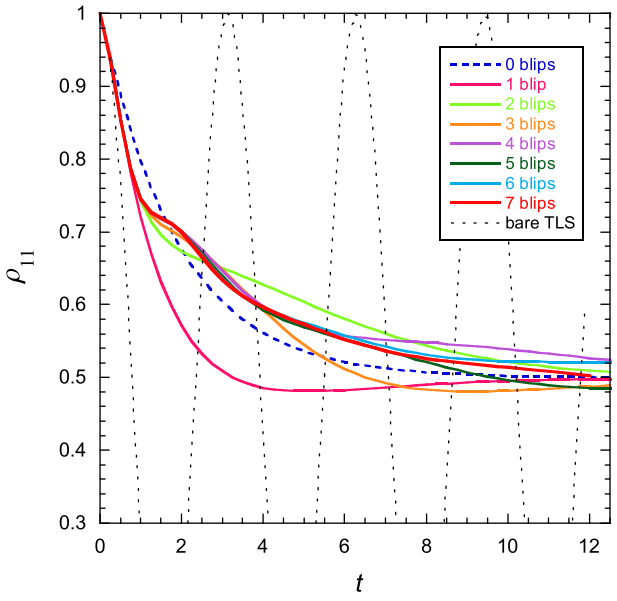

Figure 6. TLS population obtained by the blip sum method in the case of a slow, strongly coupled bath. The system was propagated for $N = 50$ path integral time steps with $\Omega\Delta t = 0.25$. The dashed blue line shows the fully incoherent result. The heavy red line shows the converged results with 7 blips. The oscillatory, short-dashed black line shows the bare TLS evolution.

segments. While the majority of them are expected to carry negligible weight, a fair number of these will be statistically significant and thus must be included. (The number of statistically significant paths varies greatly with system/bath parameters and total propagation time; typical numbers we have encountered are $10^5 - 10^{10}$.) The blip sum achieves the full sojourn sum result via a single term. Thus, the blip sum method can be viewed as a path filtering procedure with efficiency increased by many orders of magnitude. Last, the blip sum method eliminates the need for stepwise filtering, is easy to code, and has extremely low memory requirements. Its extension to an iterative algorithm seems relatively straightforward.

A very attractive possibility is to generalize the blip sum ideas described in this section to anharmonic environments treated via classical trajectories. Such a procedure could lead to a dramatic increase in efficiency of QCPI calculations.

7. Concluding remarks

Condensed phase environments can alter drastically the time evolution of a small molecular system via dephasing processes that tend to decohere the dynamics. Within the path integral formulation of time-dependent quantum mechanics, all decoherence effects from the system's environment are included in the influence functional. Under certain conditions that are favored when the interaction between system and solvent is diluted over a large number of degrees of freedom, all terms in the influence functional beyond quadratic order vanish and the influence functional takes a Gaussian form. In that case, the effects on the quantum system by its complex environment are identical to those from a fictitious harmonic bath that produces an influence functional identical to that of the polyatomic medium. The frequencies and coupling parameters of this fictitious, temperature-dependent harmonic bath can be obtained from the force autocorrelation function of the polyatomic environment, which is usually obtained from molecular dynamics calculations. A powerful iterative path integral methodology for propagating the system's reduced density matrix has been available since the mid-1990s. This proceeds via an iterative procedure that treats simultaneously all coordinates of system paths that span the memory or decoherence time length. The iterative nature of that algorithm implies linear scaling with the total propagation time, but the full propagator is a tensor of rank determined by the number of time steps required to span the memory length. Path filtering and path integral renormalization procedures can dramatically decrease the computational effort required to treat strongly-coupled long-memory baths.

Examination of the influence functional from a harmonic bath reveals two distinct decoherence mechanisms. The first, 'classical' mechanism, is the only decoherence process that survives at high temperatures and causes direct damping. This mechanism arises from classical trajectories of the isolated environment, which 'drive' the system, causing the absorption and emission of phonons. As a result, its effects on the evolution of the system can be captured by inexpensive memory-free procedures. The second, 'quantum' decoherence mechanism, originates from back-reaction effects and is associated with spontaneous phonon emission. Further, enforcing zero-point energy via proper quantization of the thermal density allows the most significant portion of the quantum decoherence process to be accounted for by the classical mechanism. Since each system path gives rise to distinct solvent trajectories, the quantum decoherence mechanism cannot be mapped on a time-dependent Schrödinger equation and thus cannot be accounted for by simple Markovian procedures. At high temperatures and/or weak system-solvent interaction, the effects of the quantum system on the high-energy trajectories of the solvent is relatively minor, making the quantum decoherence process insignificant. As the temperature is lowered, the classical decoherence process gradually ceases to dominate the dynamics, such that significant corrections to the population evolution may arise from the quantum decoherence mechanism. Interestingly, it was seen that even at low temperature and moderately strong system-bath interaction the classical decoherence process plays a very prominent role on the dynamics of a quantum system. Taking advantage of these ideas has recently led to an accurate and efficient QCPI algorithm.

Another important consequence of classical decoherence is the shortening of the system's quantum interference path pairs or blips. Low-frequency baths often lead to long memory effects, which pose a challenge to path integral methods. However, a small number of blips often dominates the dynamics in these cases. An efficient, time-local procedure for performing the blip sum was introduced, which avoids enumeration of large numbers of long sojourn segments.

In summary, classical decoherence generally plays the most important role on the dynamics of a system interacting with a condensed phase environment. Classical decoherence processes can be exploited in multiple ways to enable path integral calculations in regimes where the required number of terms is astronomical. On the other hand, quantum decoherence introduces nonlocal effects to the dynamics. Fortunately, its effects are subtle and often relatively minor, allowing efficient treatments.

Acknowledgment

This material is based upon work supported by the National Science Foundation under Award CHE 11-12422.

References

[1] A.O. Caldeira, A.J. Leggett, Phys. A 121 (1983) 587.
[2] U. Weiss, Quantum Dissipative Systems, World Scientific, Singapore, 1993.
[3] R.A. Marcus, N. Sutin, Biochim. Biophys. Acta 811 (1985) 265.
[4] N. Makri, J. Phys. Chem. 103 (1999) 2823.
[5] R.P. Feynman, Rev. Mod. Phys. 20 (1948) 367.
[6] R.P. Feynman, A.R. Hibbs, Quantum Mechanics and Path Integrals, McGraw-Hill, New York, 1965.
[7] R.P. Feynman, F.L. Vernon, Ann. Phys. 24 (1-2) (1963) 118.
[8] A.J. Leggett, S. Chakravarty, A.T. Dorsey, M.P.A. Fisher, A. Garg, M. Zwerger, Rev. Mod. Phys. 59 (1987) 1.
[9] R. Zwanzig, J. Stat. Phys. 9 (1973) 215.
[10] C.H. Mak, D. Chandler, Phys. Rev. A 44 (1991) 2352.
[11] R. Egger, C.H. Mak, Phys. Rev. B 50 (1994) 15210.
[12] N. Metropolis, A.W. Rosenbluth, M.N. Rosenbluth, H. Teller, E. Teller, J. Chem. Phys. 21 (1953) 1087.
[13] V.S. Filinov, Nucl. Phys. B 271 (1986) 717.
[14] N. Makri, W.H. Miller, Chem. Phys. Lett. 139 (1987) 10.
[15] N. Makri, W.H. Miller, J. Chem. Phys. 89 (1988) 2170.
[16] J.D. Doll, D.L. Freeman, M.J. Gillan, Chem. Phys. Lett. 143 (1988) 277.
[17] J.D. Doll, D.L. Freeman, Adv. Chem. Phys. 73 (1988) 289.
[18] C.H. Mak, R. Egger, J. Chem. Phys. 110 (1999) 12.
[19] R. Egger, L. Muhlbacher, C.H. Mak, Phys. Rev. E 61 (2000) 5961.
[20] D.E. Makarov, N. Makri, Chem. Phys. Lett. 221 (1994) 482.
[21] N. Makri, D.E. Makarov, J. Chem. Phys. 102 (1995) 4600.
[22] N. Makri, D.E. Makarov, J. Chem. Phys. 102 (1995) 4611.
[23] N. Makri, J. Math. Phys. 36 (1995) 2430.
[24] E. Sim, N. Makri, Comp. Phys. Commun. 99 (1997) 335.
[25] N. Makri, J. Phys. Chem. 102 (1998) 4414.
[26] J. Shao, N. Makri, Chem. Phys. 268 (2001) 1.
[27] J. Shao, N. Makri, J. Chem. Phys. 116 (2002) 507.
[28] N. Makri, Chem. Phys. Lett. 193 (1992) 435.
[29] M. Topaler, N. Makri, Chem. Phys. Lett. 210 (1993) 285.
[30] J.V. Lill, G.A. Parker, J.C. Light, Chem. Phys. Lett. 89 (1982) 483.
[31] J. Echave, D.C. Clary, J. Chem. Phys. 190 (1992) 225.
[32] M. Topaler, N. Makri, Chem. Phys. Lett. 210 (1993) 448.
[33] N. Makri, Chem. Phys. Lett. 159 (1989) 489.
[34] N. Makri, J. Phys. Chem. 97 (1993) 2417.
[35] E. Sim, N. Makri, Chem. Phys. Lett. 249 (1996) 224.
[36] E. Sim, J. Chem. Phys. 115 (2001) 4450.
[37] R. Lambert, N. Makri, Mol. Phys. 110 (2012) 1967.
[38] A.A. Golosov, R.A. Friesner, P. Pechukas, J. Chem. Phys. 110 (1999) 138.
[39] A.A. Golosov, R.A. Friesner, P. Pechukas, J. Chem. Phys. 112 (2000) 2095.

[40] N. Makri, Mol. Phys. 110 (2012) 1001.
[41] T.C. Berkelbach, D.R. Reichman, T.E. Markland, J. Chem. Phys. 136 (2012) 034113.
[42] T.C. Berkelbach, T.E. Markland, D.R. Reichman, J. Chem. Phys. 136 (2012) 084104.
[43] D. Segal, A.J. Millis, D.R. Reichman, Phys. Rev. B 82 (2010) 205323.
[44] L. Simine, D. Segal, J. Chem. Phys. 138 (2013) 214111.
[45] N. Makri, J. Chem. Phys. 111 (1999) 6164.
[46] G. Ilk, N. Makri, J. Chem. Phys. 101 (1994) 6708.
[47] K. Forsythe, N. Makri, Phys. Rev. B 60 (1999) 972.
[48] S. Weiss, J. Eckel, M. Thorwart, R. Egger, Phys. Rev. B 77 (2008) 195316.
[49] A. Ishizaki, Y. Tanimura, J. Phys. Soc. Jpn 74 (12) (2005) 3131.
[50] Y. Tanimura, J. Phys. Soc. Jpn. 75 (2006) 082001.
[51] N. Makri, J. Chem. Phys. 109 (1998) 2994.
[52] M. Berkowitz, C.L. Brooks, S.A. Adelman, J. Chem. Phys. 72 (1980) 3889.
[53] R. Lambert, N. Makri, J. Chem. Phys. 137 (2012) 22A552.
[54] R. Lambert, N. Makri, J. Chem. Phys. 137 (2012) 22A553.
[55] N. Makri, K. Thompson, Chem. Phys. Lett. 291 (1998) 101.
[56] K. Thompson, N. Makri, J. Chem. Phys. 110 (1999) 1343.
[57] Q. Shi, E. Geva, J. Chem. Phys. 121 (2004) 3393.
[58] T. Banerjee, N. Makri, J. Phys. Chem. 117 (2013) 13357.
[59] W.H. Miller, Adv. Chem. Phys. 30 (1975) 77.
[60] X. Sun, H. Wang, W.H. Miller, J. Chem. Phys. 109 (1998) 4190.
[61] H. Wang, M. Thoss, K.L. Sorge, R. Gelabert, X. Gimenez, W.H. Miller, J. Chem. Phys. 114 (2001) 2562.
[62] J. Ray, N. Makri, J. Phys. Chem. 103 (1999) 9417.
[63] L.S. Schulman, Techniques and Applications of Path Integration, John Wiley and Sons, New York, 1981.
[64] R.P. Feynman, J.F.L. Vernon, Ann. Phys. 24 (1963) 118.
[65] N. Makri, Phys. Chem. Chem. Phys. 13 (32) (2011) 14442.
[66] M.R. Hermes, M. Keceli, S. Hirata, J. Chem. Phys. 136 (2012) 234109.
[67] K. Binder, D.W. Heermann, Monte Carlo Simulation in Statistical Physics, Springer-Verlag, 1988.
[68] J.D. Doll, D.L. Freeman, T.L. Beck, Adv. Chem. Phys. 78 (1990) 61.
[69] N. Makri, Comp. Phys. Comm. 63 (1991) 389.
[70] D. Thirumalai, E.J. Bruskin, B.J. Berne, J. Chem. Phys. 79 (1983) 5063.
[71] M.F. Trotter, Proc. Am. Math. Soc. 10 (1959) 545.
[72] T. Holstein, Ann. Phys. 8 (1959) 343.
[73] M. Topaler, N. Makri, J. Chem. Phys. 101 (1994) 7500.
[74] M. Topaler, N. Makri, J. Phys. Chem. 100 (1996) 4430.
[75] N. Makri, E. Sim, D.E. Makarov, M. Topaler, Proc. Natl. Acad. Sci. USA 93 (1996) 3926.
[76] E. Sim, N. Makri, J. Phys. Chem. 101 (1997) 5446.
[77] M. Thorwart, E. Paladino, M. Grifoni, Chem. Phys. 296 (2004) 333.
[78] R.D. Coalson, D.G. Evans, Chem. Phys. 296 (2004) 117.
[79] X.-T. Liang, Phys. C 442 (2006) 79.
[80] H. Kim, O. Choi, E. Sim, J. Phys. Chem. 114 (2010) 20394.
[81] H. Kim, E. Sim, J. Phys. Chem. 114 (2010) 1312.
[82] E.A. Polyakov, A.P. Lyubartsev, P.N. Vorontsov-Velyaminov, J. Chem. Phys. 133 (2010) 194103.
[83] M. Sahrapour, N. Makri, J. Chem. Phys. 132 (2010) 134506.
[84] P. Nalbach, M. Thorwart, Chem. Phys. 375 (2010) 234.
[85] P. Nalbach, D. Braun, M. Thorwart, Phys. Rev. E 84 (2011) 041926.
[86] M. Glässl, A. Vagov, S. Lüker, D.E. Reiter, M.D. Croitoru, P. Machnikowski, V.M. Axt, T. Kuhn, Phys. Rev. B 84 (2011) 195311.
[87] X. Zhong, Y. Zhao, J. Chem. Phys. 135 (2011) 134110.
[88] J.-C. Lee, O. Choi, E. Sim, J. Phys. Chem. Lett. 3 (2012) 714.
[89] M. Sahrapour, N. Makri, J. Chem. Phys. 138 (2013) 114109.
[90] D.E. Makarov, N. Makri, Phys. Rev. E 52 (1995) 5863.
[91] N. Makri, J. Chem. Phys. 106 (1997) 2286.
[92] G. Taft, N. Makri, J. Phys. B 31 (1998) 209.
[93] M. Thorwart, P. Reimann, P. Hänggi, Phys. Rev. E 62 (2000) 5808.
[94] K. Dong, N. Makri, Phys. Rev. A 70 (2004) 042101.
[95] E.J. Wigner, Chem. Phys. 5 (1937) 720.
[96] N. Makri, J. Shao, Chemie 214 (2000) 1187.
[97] H. Wang, X. Sun, W.H. Miller, J. Chem. Phys. 108 (1998) 9726.
[98] J.A. Poulsen, G. Nyman, P.J. Rossky, J. Chem. Phys. 119 (23) (2003) 12179.
[99] M.F. Herman, E. Kluk, Chem. Phys. 91 (1984) 27.
[100] A. Nakayama, N. Makri, Proc. Nat. Acad. Sci. USA 102 (2005) 4230.
[101] N. Makri, W.H. Miller, J. Chem. Phys. 116 (2002) 9207.
[102] J.C. Tully, J. Chem. Phys. 93 (1990) 1061.
[103] S. Hammes-Schiffer, J.C. Tully, J. Chem. Phys. 101 (1994) 4657.
[104] K. Thompson, N. Makri, Phys. Rev. E 59 (1999) R4729.
[105] J. Shao, N. Makri, J. Phys. Chem. A 103 (1999) 7753.
[106] H. Wang, D.E. Manolopoulos, W.H. Miller, J. Chem. Phys. 115 (2001) 6317.
[107] R. Gelabert, X. Gimenez, M. Thoss, H. Wang, W.H. Miller, J. Chem. Phys. 114 (2001) 2572.

Nancy Makri obtained a B.S. from the University of Athens in 1985 and a Ph.D. from the University of California at Berkeley in 1989. After spending two years as a Junior Fellow at Harvard, she joined the Chemistry faculty of the University of Illinois, where she is currently the E.W. and J.M. Gutgsell Professor of Chemistry and Physics. Makri's research focuses on the development of theoretical methods for simulating the quantum dynamics of condensed phase processes. Makri is an APS Fellow and the recipient of the 2000 Bodossaki Academic Prize in Physical Sciences. She is also a member and the 1995 Medalist of the International Academy of Quantum Molecular Science.